JAST, Vol. 12, No. 2, pp. 1-9

JAST Journal of Aerospace Science and Technology

Analytical and Numerical Investigation of Parameters Effective on Energy Absorption Circular Composite Tube under Internal and Axial Pressure

M. Noorabadi[1], M. Rahnama[2], M.A. Ghasemi[3], J. Eskandari Jam[4]

1-4. Composite Materials & Technology Center, Malek-Ashtar University of Technology, Tehran, Iran

eskandari@mut.ac.ir

In this paper, the energy absorption capacity of stiffened circular composite tube is considered. The governing equations and dynamic equilibrium are first derived and then solved. Additionally, a finite element model of reinforced circular composite tube structure is modeled. In the following, the effects of various parameters such as structural geometry, number of rings and stingers on the mechanical behavior of such tubes are considered. The stiffened cylinder is under axial loading and internal pressure, and boundary conditions for both sides of the cylinder are considered as simple supports. Results show an increase in the amount of energy in the stingers when the number of stingers rise, and a decrease in the total amount of energy when the number of rings and stringers soar. Total strain energy and the strain energy created in structural elements rise by increasing the ratio of radius to thickness. The analytical solution results are in good compatibility with the results achieved from the finite element method.

Keywords:Energy, Finite element, Rings, Stringers, Deflection

Introduction

Reinforced circular tubes are widely used in engineering design. Their application manifests itself particularly in aerospace structures. These types of structures are employed for manufacturing the main parts of airplanes, missiles, rockets, etc. Many efforts have been made over recent years in different engineering areas regarding the behavior investigation of these structures. Meanwhile, studying the dynamic and vibrating behavior of cylindrical structures is one of the fields most focused on in engineering. Energy absorption elements are widely used in various structures for the sake of their protection. These elements are made of different materials like metals, forms and composites. Absorption properties of composite materials cause them to be noticed by many designers in automobile and aircraft manufacturing industries.

Egle and Dewall [1] consider the influence of stiffeners on natural frequency changes of ring-and-stringer stiffened circular cylindrical shells with different types of end conditions. The stiffeners are treated as discrete elements and energy method and Hamilton's principle are employed to derive their equations of motion. Mustafa and Ali [2] used an energy method to analyze free vibration of stiffened circular cylindrical shells considering bending, tension and torsion of the stiffeners. Kim and Lee [3] performed a transient analysis on ring stiffened composite cylindrical shell. The use of annular 3D textiles as reinforcer in polymer composites was developed by Verpoest et al. [4] in the early 1990s. Phillips et al. [5] also reported higher energy absorption capacity and less specific compressive strength and bending stiffness of such

1. M. Sc.
2. M. Sc.
3. M. Sc.
4. Professor (Corresponding Authore)

composites compared with sandwich polymer composites. Yu et al. [6] studied the energy absorption characteristics of grid-domed 3D structures under semi static and impact forms of pressure. In 1973, Herald [7] tested a structure considering the optimum design. Results showed that the energy absorption value of composites such as carbon-epoxy fall within 50-80 K_J / K_g [8], but the values could be increased to 110 K_J / K_g [9]. Barant et al. [10] considered the application of composites in impacting energy absorption. Results showed that energy absorption is especially important for foam-filled elements. Michell Hoo Fat et al. [11] predicted the energy absorption value of metal-glass/epoxy laminate using energy method.

Sun et al. [12] considered energy absorption in aluminum-carbon sandwich panel with short kevlar-fiber reinforcement. Wang et al. [13] considered energy absorption properties of multi-layered corrugated paperboard. Ma et al. [14] also conducted a study on the energy absorption properties of carbon-aramid fiber filament winding composite tube. Results showed a better energy absorption for 3-layered aramid-carbon-aramid structure in comparison with 5-layered aramid-carbon-aramid-carbon-aramid structure.

In this paper, the energy absorption capacity of stiffened circular composite tubes is considered. The governing equations are first derived, and then, a finite element model of the structure is established, followed by numerical analysis on energy absorption of the structure through alternation of different parameters.

Governing equations

Displacement vector components of cylindrical shells according to classic model and assuming Donnell theorem are described as the expression below:

$$u_1(x,y,z) = u(x,y) - z\frac{\partial w}{\partial x},$$
$$u_2(x,y,z,t) = v(x,y) - z\frac{\partial w}{\partial y}, \quad (1)$$
$$u_3(x,y,z,t) = w(x,y).$$

In Eq. (1), planner displacement components in X and Y direction are shown by *u(x,y)* and *v(x,y)* respectively. *w(x,y)* is also radial displacement. The distance between each point of the plate and the Bending plane is expressed by *z*.

Changes of a strain energy, *U*, of an elastic body is:

$$\delta U = \int_{\Omega} \sigma_{ij}\delta\varepsilon_{ij} d\Omega \quad (2)$$

σ_{ij} and $\delta\varepsilon_{ij}$ parameters are the Cauchy stress tensor, $\bar{\boldsymbol{\sigma}}$, and the changes of strain tensor, $\boldsymbol{\delta\bar{\varepsilon}}$, respectively. Additionally, nonzero components of the strain according to classic Donnell for cylindrical shells are as follows:

$$\varepsilon_{11} = \frac{\partial u}{\partial x} - z\frac{\partial^2 w}{\partial x^2}$$
$$\varepsilon_{22} = \frac{\partial y}{\partial y} + \frac{w}{R} - z\frac{\partial^2 w}{\partial y^2} \quad (3)$$
$$2\varepsilon_{12} = \frac{\partial u}{\partial y} + \frac{\partial v}{\partial x} - 2z\frac{\partial^2 w}{\partial x \partial y}$$

In real practical conditions, there is no constraint applied on *h*, i.e. the thickness of the plate, for it to remain without any changes or to ensure the absence of axial strain ε_{33} in thickness direction. Besides, the practical condition of normal traction forces on both upper and lower surfaces of the plate are negligible or would vanish. As a result and due to the assumption of a small thickness for the plate, the stress component σ_{33} is negligible at all points of the plane in comparison with other stress components; therefore, plane stress and strain constitutive equations are applied for deduction of relations as below. For layered composite materials, the constitutive equations for each layer in such a state are expressed as below:

$$\begin{Bmatrix}\sigma_{11}\\ \sigma_{22}\\ \sigma_{12}\end{Bmatrix} = \bar{\mathbf{Q}}_k(\theta)\begin{Bmatrix}\varepsilon_{11}\\ \varepsilon_{22}\\ 2\varepsilon_{12}\end{Bmatrix}; \quad (4)$$
$$\bar{\mathbf{Q}}_k(\theta) = \left[\mathbf{H}(\theta_k)\right]^T \mathbf{Q}\,\mathbf{H}_k(\theta_k)$$

Where $\bar{\boldsymbol{Q}}_{\boldsymbol{4}}$ is the stiffness matrix at main coordinates and $\boldsymbol{H_k(\theta)}$ is the transfer matrix for each layer and is defined as:

$$\mathbf{Q} = \begin{bmatrix} \frac{E_1}{1-\nu_{12}\nu_{21}} & \frac{\nu_{12}E_1}{1-\nu_{12}\nu_{21}} & 0 \\ \frac{\nu_{12}E_1}{1-\nu_{12}\nu_{21}} & \frac{E_2}{1-\nu_{12}\nu_{21}} & 0 \\ 0 & 0 & G_{12} \end{bmatrix} \quad (5)$$

and

$$\mathbf{H}(\theta_k) = \begin{bmatrix} Cos^2(\theta_k) & Sin^2(\theta_k) & Sin(2\theta_k) \\ Sin^2(\theta_k) & Cos^2(\theta_k) & -Sin(2\theta_k) \\ -\frac{Sin(2\theta_k)}{2} & \frac{Sin(2\theta_k)}{2} & Cos(2\theta_k) \end{bmatrix}$$

Equation of longitudinal and circumferential stiffeners

Since the shell in the stiffeners behaves as a continuum in a proper and ideal practical situation, the displacements in stiffeners can be expressed as:

$$u_s = u - z\frac{\partial w}{\partial x}$$
$$v_s = u - z\frac{\partial w}{\partial y} \quad (6)$$
$$w_s = w(x,y)$$

The strain energy in longitudinal stiffeners (stringers) is expressed as:

$$U_s = \sum_{K=1}^{N_s} \frac{b_{sk}}{2} E_{sk} \int_0^L \int_{R+h/2}^{R+h/2+h_{sk}} \varepsilon_{ss}^2 dz dx \quad (7)$$

In Eq. (6), E_{sk}, b_{sk} and h_{sk} show the modulus of elasticity, width, and thickness, respectively. The energy that is stored in circumferential stiffeners (rings) is expressed as:

$$U_R = \sum_{K=1}^{N_r} \frac{1}{2} E_{rk} \int_0^{2\pi R+h/2+h_r} \int_{R+h/2} \varepsilon_{rr}^2 dA_k dy \quad (8)$$

$$Where \quad \varepsilon_{rr} = \frac{dv}{dy} + \frac{w}{R} - z\frac{\partial^2 w}{\partial y^2}$$

Equations governing static equilibrium

In order to formulate the governing equations and static equilibrium, changes in energy and external work done by axial traction are calculated first, and the governing equations are then derived through replacing them into minimum total potential energy principle. For this purpose, changes in cylindrical shell strain energy are to be equal to:

$$\delta U_\varepsilon = \int_A P dx dy \quad (9)$$

In the above equation:

$$\mathrm{P} = -M_{11}\frac{\partial^2(\delta w)}{\partial x^2} - M_{22}\frac{\partial^2(\delta w)}{\partial y^2} - 2M_{12}\frac{\partial^2(\delta w)}{\partial x \partial y} + \frac{N_{22}}{R}\delta w + N_{11}\frac{\partial(\delta u)}{\partial x} + N_{22}\frac{\partial(\delta v)}{\partial y} + N_{12}\left(\frac{\partial(\delta u)}{\partial y} + \frac{\partial(\delta v)}{\partial x}\right) \quad (10)$$

Twice integrations of the above equation by parts:

$$\delta U_\varepsilon = \int_A \delta U^{\text{int}}\, dA + \left[\int_{y=0}^{y=2\pi R} \delta U^{bound}\, dy\right]_{x=0}^{x=L} \quad (11)$$

Where:

$$\delta U^{\text{int}} : -\left[\frac{\partial^2 M_{11}}{\partial x^2} + \frac{\partial^2 M_{22}}{\partial y^2} + 2\frac{\partial^2 M_{12}}{\partial x \partial y} - \frac{N_{22}}{R}\right]\delta w - \left[\frac{\partial N_{11}}{\partial x} + \frac{\partial N_{12}}{\partial y}\right]\delta u - \left[\frac{\partial N_{22}}{\partial y} + \frac{\partial N_{12}}{\partial x}\right]\delta v, \quad (12)$$

$$\delta U^{bound} = N_{11}\delta u + N_{12}\,\delta v + \left[\frac{\partial M_{11}}{\partial x} + 2\frac{\partial M_{12}}{\partial y}\right]\delta w - M_{11}\delta\left(\frac{\partial w}{\partial x}\right), \quad (13)$$

Stored strain energy change in longitudinal stiffeners is expressed as below:

$$\delta U_S = \frac{E_s}{d_s}\int_0^{2\pi R}\int_0^L \left[A_s\frac{\partial u}{\partial x}\delta\left(\frac{\partial u}{\partial x}\right) + I_{0s}\frac{\partial^2 w}{\partial x^2}\delta\left(\frac{\partial^2 w}{\partial x^2}\right) - Q_s\left(\frac{\partial u}{\partial x}\delta\left(\frac{\partial^2 w}{\partial x^2}\right) + \frac{\partial^2 w}{\partial x^2}\delta\left(\frac{\partial u}{\partial x}\right)\right)\right] dx dy \quad (14)$$

Stored strain energy change in circumferential stiffeners is also expressed as:

$$\delta U_R = \frac{E_r}{d_r}\int_0^{2\pi R}\int_0^L \left[A_r\left(\frac{\partial v}{\partial y} + \frac{w}{R}\right)\delta\left(\frac{\partial v}{\partial y} + \frac{w}{R}\right) + I_{0r}\frac{\partial^2 w}{\partial y^2}\delta\left(\frac{\partial^2 w}{\partial y^2}\right) - Q_r\left(\frac{\partial v}{\partial y} + \frac{w}{R}\right)\delta\left(\frac{\partial^2 w}{\partial y^2}\right) - Q_r\frac{\partial^2 w}{\partial y^2}\delta\left(\frac{\partial v}{\partial y} + \frac{w}{R}\right)\right] dx dy \quad (15)$$

Change of external work done, δW, is calculated as:

$$\delta W_a = -\int_0^{2\pi R}\int_0^L N_a\frac{\partial^2 w}{\partial x^2}\delta w\, dx\, dy + \int_0^{2\pi R} N_a\frac{\partial w}{\partial x}\delta w dy\Big|_{x=0}^{x=L} \quad (16)$$

Minimum total potential energy principle is stated as:

$$\delta\left(U_\varepsilon + U_s + U_r - W\right) = 0. \quad (17)$$

Replacing the changes in summation of the strain energy and the work done by external forces

into Eq. (17), the governing equations on static equilibrium using Donnell theory become:

δu:

$$\frac{\partial N_{11}}{\partial x}+\frac{\partial N_{12}}{\partial y}+\frac{E_s}{d_s}\left(A_s\frac{\partial^2 u}{\partial x^2}-Q_s\frac{\partial^3 w}{\partial x^3}\right)=0,$$

δv:

$$\frac{\partial N_{12}}{\partial x}+\frac{\partial N_{22}}{\partial y}+\frac{E_r}{d_r}\left(A_r\frac{\partial}{\partial y}\left(\frac{\partial v}{\partial y}+\frac{w}{R}\right)-Q_r\frac{\partial^3 w}{\partial y^3}\right)=0 \quad (18)$$

The boundary conditions at both ends of the shell $x=0, L$ are expressed as:

$$I_{11}+\frac{E_s}{d_s}\left(A_s\frac{\partial u}{\partial x}-Q_s\frac{\partial^2 w}{\partial x^2}\right)=0,\quad or\quad \delta u=0,$$

$$N_{12}=0,\quad or\quad \delta v=0,$$

$$\frac{\partial M_{11}}{\partial x}+2\frac{\partial M_{12}}{\partial y}-\frac{E_s}{d_s}\left(I_{0s}\frac{\partial^3 w}{\partial x^3}-Q_s\frac{\partial^2 u}{\partial x^2}\right)=0,\quad or\quad \delta w=0\ , \quad (19)$$

$$M_{11}-\frac{E_s}{d_s}\begin{pmatrix} I_{0s}\dfrac{\partial^2 w}{\partial x^2} \\ -Q_s\dfrac{\partial u}{\partial x}\end{pmatrix}=0,\quad or\quad \delta\left(\frac{\partial w}{\partial x}\right)=0$$

Solving the Equations

In order to solve the governing equations, cinematic components of displacement vector can be expressed as:

$$u(x,y)=\sum_{n=1}^{\infty}\sum_{m=1}^{\infty}u_{mn}\ \cos\left(\frac{m\pi}{L}x\right)\sin\left(\frac{n}{2R}y\right),$$
$$v(x,y)=\sum_{n=1}^{\infty}\sum_{m=1}^{\infty}v_{mn}\ \sin\left(\frac{m\pi}{L}x\right)\cos\left(\frac{n}{2R}y\right), \quad (20)$$
$$w(x,y)=\sum_{n=1}^{\infty}\sum_{m=1}^{\infty}w_{mn}\ \sin\left(\frac{m\pi}{L}x\right)\sin\left(\frac{n}{2R}y\right).$$

For internal pressure:

$$P_{in}=\sum_{n=1}^{\infty}\sum_{m=1}^{\infty}\mathrm{P}_{mn}\ \sin\left(\frac{m\pi}{L}x\right)\sin\left(\frac{n}{2R}y\right) \quad (21)$$

In the above equation:

$$\mathrm{P}_{mn}=\frac{16P_{in}}{mn\pi^2}\quad for\ n,m=1,3,..... \quad (22)$$

With placement of cinematic components series (Eq. (20)) and internal pressure (Eq. (21)) in governing equations:

$$\begin{pmatrix} g_{11} & g_{12} & g_{13}\\ g_{12} & g_{22} & g_{23}\\ g_{13} & g_{23} & g_{33}\end{pmatrix}\begin{Bmatrix} u_{mn}\\ v_{mn}\\ w_{mn}\end{Bmatrix}=\begin{Bmatrix} 0\\ 0\\ \mathrm{P}_{mn}\end{Bmatrix}, \quad (23)$$

where g_{ij} is defined as:

$$g_{11}=\left(A_{11}+\frac{E_sA_s}{d_s}\right)\left(\frac{m\pi}{L}\right)^2+A_{66}\left(\frac{n}{2R}\right)^2,$$
$$g_{12}=(A_{12}+A_{66})\left(\frac{m\pi}{L}\right)\left(\frac{n}{2R}\right),$$
$$g_{13}=-\left(\frac{A_{12}}{R}+\frac{E_sQ_s}{d_s}\left(\frac{m\pi}{L}\right)^2\right)\left(\frac{m\pi}{L}\right),$$
$$g_{22}=A_{66}\left(\frac{m\pi}{L}\right)^2+\left(A_{22}+\frac{E_rA_r}{d_r}\right)\left(\frac{n}{2R}\right)^2,$$
$$g_{23}=-\left(A_{22}+\frac{E_rA_r}{d_r}\right)\left(\frac{n}{2R^2}\right)-\frac{E_rQ_r}{d_r}\left(\frac{n}{2R}\right)^3,$$
$$g_{33}=\left(D_{11}+\frac{E_sI_{0s}}{d_s}\right)\left(\frac{m\pi}{L}\right)^4$$
$$g_{11}=\left(A_{11}+\frac{E_sA_s}{d_s}\right)\left(\frac{m\pi}{L}\right)^2+A_{66}\left(\frac{n}{2R}\right)^2,$$
$$g_{12}=(A_{12}+A_{66})\left(\frac{m\pi}{L}\right)\left(\frac{n}{2R}\right), \quad (24)$$
$$g_{13}=-\left(\frac{A_{12}}{R}+\frac{E_sQ_s}{d_s}\left(\frac{m\pi}{L}\right)^2\right)\left(\frac{m\pi}{L}\right),$$
$$g_{22}=A_{66}\left(\frac{m\pi}{L}\right)^2+\left(A_{22}+\frac{E_rA_r}{d_r}\right)\left(\frac{n}{2R}\right)^2,$$
$$g_{23}=-\left(A_{22}+\frac{E_rA_r}{d_r}\right)\left(\frac{n}{2R^2}\right)-\frac{E_rQ_r}{d_r}\left(\frac{n}{2R}\right)^3,$$
$$g_{33}=\left(D_{11}+\frac{E_sI_{0s}}{d_s}\right)\left(\frac{m\pi}{L}\right)^4$$
$$+\left(D_{22}+\frac{E_rI_{0r}}{d_r}\right)\left(\frac{n}{2R}\right)^4+\frac{1}{R^2}\left(A_{22}+\frac{E_rA_r}{d_rR}\right)$$
$$+2\left(D_{12}+2D_{66}\right)\left(\frac{m\pi}{L}\right)^2\left(\frac{n}{2R}\right)^2$$
$$+\frac{E_rQ_r}{d_rR}\left(\frac{n}{2R}\right)^2-N_a\left(\frac{m\pi}{L}\right)^2,$$

Employing Cramer's rule in the order of equations system solution, Fourier coefficients are obtained as follows:

$$\left(u_{mn}, v_{mn}, w_{mn}\right) = \frac{\mathrm{P}_{mn}}{\Delta_{mn}}\left(\Delta^{u}_{mn}, \Delta^{v}_{mn}, \Delta^{w}_{mn}\right)$$

$$\Delta_{mn} = \begin{vmatrix} g_{11} & g_{12} & g_{13} \\ g_{12} & g_{22} & g_{23} \\ g_{13} & g_{23} & g_{33} \end{vmatrix}, \Delta^{u}_{mn} = \begin{vmatrix} g_{12} & g_{13} \\ g_{22} & g_{23} \end{vmatrix}, \quad (25)$$

$$\Delta^{v}_{mn} = -\begin{vmatrix} g_{11} & g_{13} \\ g_{12} & g_{23} \end{vmatrix}, \Delta^{w}_{mn} = \begin{vmatrix} g_{11} & g_{12} \\ g_{12} & g_{22} \end{vmatrix}$$

Replacing Eq. (25) into Eq. (20):

$$u(x,y) = \sum_{n=1}^{\infty}\sum_{m=1}^{\infty} \frac{\Delta^{u}_{mn}}{\Delta_{mn}} \mathrm{P}_{mn} \cos(\frac{m\pi}{L}x)\sin(\frac{n}{2R}y),$$

$$v(x,y) = \sum_{n=1}^{\infty}\sum_{m=1}^{\infty} \frac{\Delta^{v}_{mn}}{\Delta_{mn}} \mathrm{P}_{mn} \sin(\frac{m\pi}{L}x)\cos(\frac{n}{2R}y), \quad (26)$$

$$w(x,y) = \sum_{n=1}^{\infty}\sum_{m=1}^{\infty} \frac{\Delta^{w}_{mn}}{\Delta_{mn}} \mathrm{P}_{mn} \sin(\frac{m\pi}{L}x)\sin(\frac{n}{2R}y).$$

Replacing the displacement components from Eq. (26) into Eq. (4), stress components are obtained as below:

$$\sigma^{(k)}_{xx} = -\bar{\mathbf{Q}}_k(\theta)\sum_{n=1}^{\infty}\sum_{m=1}^{\infty} \Lambda^{\sigma_{xx}}_{mn}(z)\sin(\frac{m\pi}{L}x)\sin(\frac{n}{2R}y),$$

$$\sigma^{(k)}_{yy} = -\bar{\mathbf{Q}}_k(\theta)\sum_{n=1}^{\infty}\sum_{m=1}^{\infty} \Lambda^{\sigma_{yy}}_{mn}(z)\sin(\frac{m\pi}{L}x)\sin(\frac{n}{2R}y), \quad (27)$$

$$\sigma^{(k)}_{xy} = \bar{\mathbf{Q}}_k(\theta)\sum_{n=1}^{\infty}\sum_{m=1}^{\infty} \Lambda^{\sigma_{xy}}_{mn}(z)\cos(\frac{m\pi}{L}x)\cos(\frac{n}{2R}y).$$

Where Fourier coefficients in Eq. (27) are defined as:

$$\Lambda^{\sigma_{xx}}_{mn}(z) = (\frac{m\pi}{L})\left(\Delta^{u}_{mn} - z\Delta^{w}_{mn}(\frac{m\pi}{L})\right)\frac{\mathrm{P}_{mn}}{\Delta_{mn}},$$

$$\Lambda^{\sigma_{yy}}_{mn}(z) = \left(\Delta^{v}_{mn}(\frac{n}{2R}) - \frac{\Delta^{w}_{mn}}{R}(1 + z\frac{n^2}{4R})\right)\frac{\mathrm{P}_{mn}}{\Delta_{mn}}, \quad (28)$$

$$\Lambda^{\sigma_{xy}}_{mn}(z) = \left(\Delta^{u}_{mn}(\frac{n}{2R}) + \Delta^{v}_{mn}(\frac{m\pi}{L}) - 2z\Delta^{w}_{mn}(\frac{m\pi}{L})(\frac{n}{2R})\right)\frac{\mathrm{P}_{mn}}{\Delta_{mn}},$$

Finite element modeling

Finite element model includes a stiffened circular tube, where the shell and stiffeners are modelled continuously. Mechanical properties of the shell are shown in Table 1. The fiber angle is considered as $[0,90,0,90]_s$.

Table 1. Mechanical properties of the cylindrical shell

E_1 (GPa)	E_2 (GPa)	ν_{12}	ν_{23}	G_{12} (GPa)	G_{12} (GPa)
43.5	11.58	0.27	0.4	3.45	4.12

Loading conditions of the circular tube are assumed as axial loading from both sides (1E9N) and internal pressure (100E6 Pascal), and the boundary conditions are for simply supported at the two ends of the tube. Also, S4R element is used to mesh the shell and B31 element for the stiffeners.

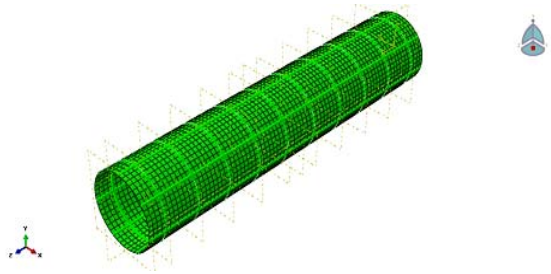

Figure 1. Meshing model of the stiffened cylinder

Verification

For a cylinder geometrical condition corresponding to Table 3, deflection and strain energy changes (Figs. 2 and 3, respectively) are derived using analytical approach.

Table 2. Geometrical characteristics of the stiffened cylinder

b_s (mm)	h_s (mm)	b_R (mm)	h_R (mm)	n_s	n_R
2	4	2	4	7	10

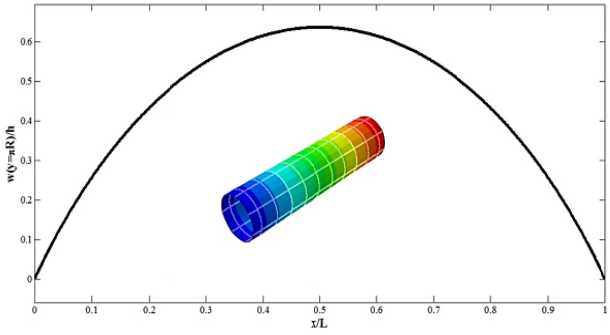

Figure 2. Deflection changes on stiffened cylinder

Table 3. Strain energy value due to [0,90,0,90]s lamination

U_shell	U_stringer	U_ring	U_total
529139.2	30.9	509.8	529650.07

Changes of total energy in stiffened cylinder structure are depicted in Fig. 3. The maximum value of total energy is 5.9e5.

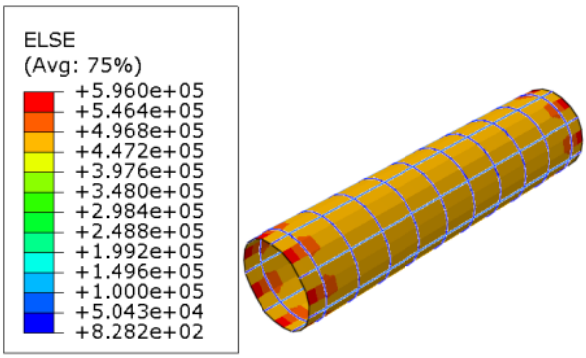

Figure 3. Total strain energy on stiffened cylinder

In Table 4, deflection and energy results obtained from analytical and numerical solutions are compared for composite cylinder. The results showed acceptable precision for the analytical solution.

Table 4. Comparison of analytical and numerical results

Method	*U_total (J)*	*Deflection (mm)*
Analytical	*5.29E5*	*5.1*
FEM	*5.96E5*	*4.9*
%	*11%*	*3%*

Analysis of results

In this section, changes of the deflection value and strain energy are considered to be due to the change in the geometrical parameters. In the stiffened cylindrical model, the thickness for each layer is considered to be 1 millimeter. The initial radius is 10 times as large as the shell thickness, the number of rings is 50, and the number of longitudinal stiffeners is 7. Boundary conditions are assumed as simple supports.

Deflection changes

Deflection changes due to changes in geometrical parameters, lamination of rings and simply supported boundary conditions are presented in the following. Normalized deflection changes in longitudinal direction of the cylinder due to strain to thickness ratio are depicted in Fig. 4. Results show that the deflection value is increased by increasing the ratio of radius to thickness at similar longitudinal positions. Deflection differences become more sharpened by increasing the radius to thickness ratio. The maximum value of deflection is observed at the middle section of the cylinder

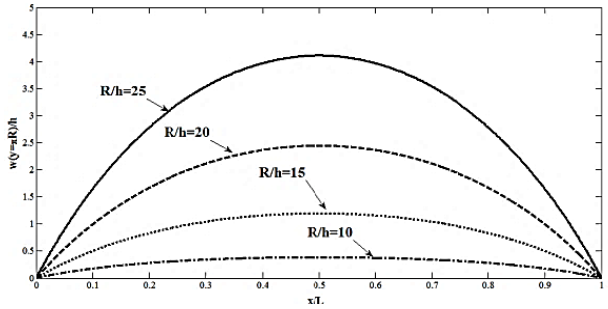

Figure 4. Normal deflection changes versus normal length ratio due to radius to shell thickness ratio

Normalized deflection changes in longitudinal direction of cylinder due to *L/R* changes are shown in Fig. 5. Results show that the deflection increases by increasing the *L/R* ratio at similar positions.

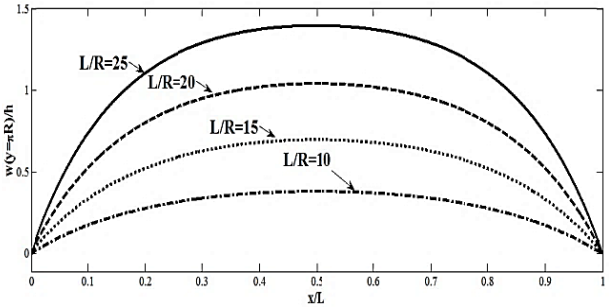

Figure 5. Normalized deflection changes versus normalized length due to changes of length to radius ratio

Results show that deflection value is decreased at similar longitudinal positions as the number of rings increases and number of stringers remains constant.

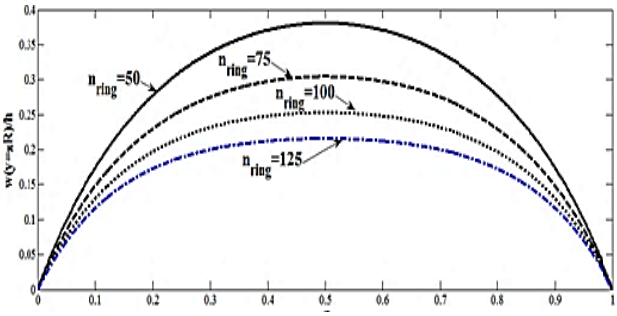

Figure 6. Normalized deflection changes versus normalized length due to change in number of rings

Energy changes

Strain energy changes due to geometrical conditions, lamination, number of rings and the stringers with simply supported boundary conditions are presented in the following.

Changes in total strain energy, longitudinal and transverse stiffeners energy and cylindrical shell energy versus cylinder radius changes are shown in the figure below. According to Fig. 6, by increasing the radius to thickness ratio, the total strain energy and the strain energy created in structural elements are increased too.

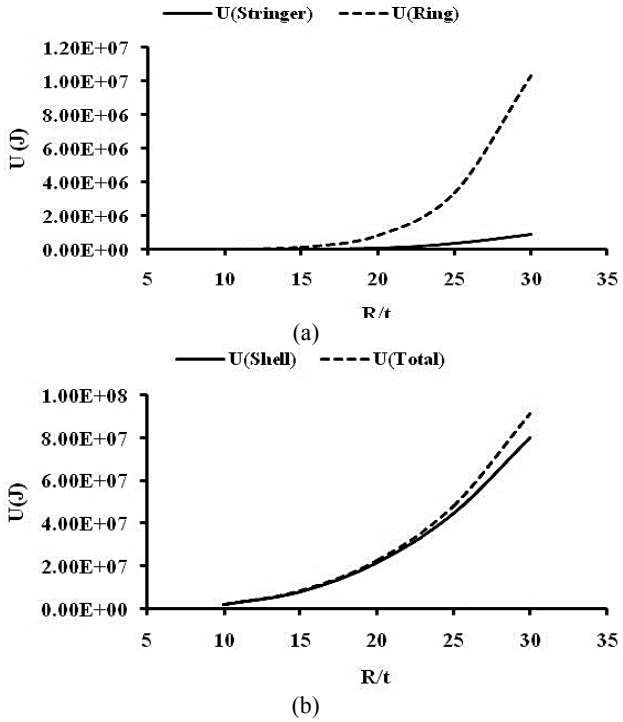

Figure 7. Changes in ring and stringer energy (a), total and shell energy (b) versus R/t ratio increase

According to Fig. 8, the strain energy in rings and stringers is increased as the ratio of length to radius increases. The total strain energy and the strain energy of the shell increase until $^{L}/_{R} = 17$ limit and decrease afterwards.

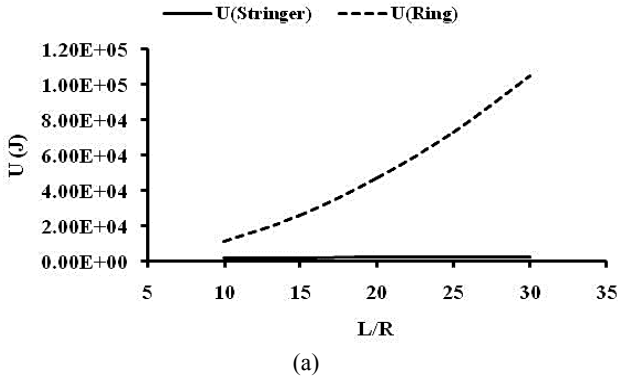

Figure 8. Changes in ring and stringer energy (a), total and shell energy (b) versus L/R ratio increase

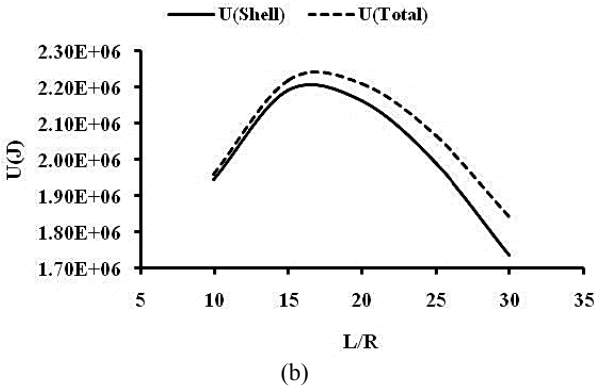

Figure 8. Changes in ring and stringer energy (a), total and shell energy (b) versus L/R ratio increase (Continuation)

Strain energy changes versus change in stiffened cylinder stringer number graph are depicted in Fig. 9. As it is evident, by increasing the number of the stringers, the energy value is increased in them while the total value of the strain energy is decreased.

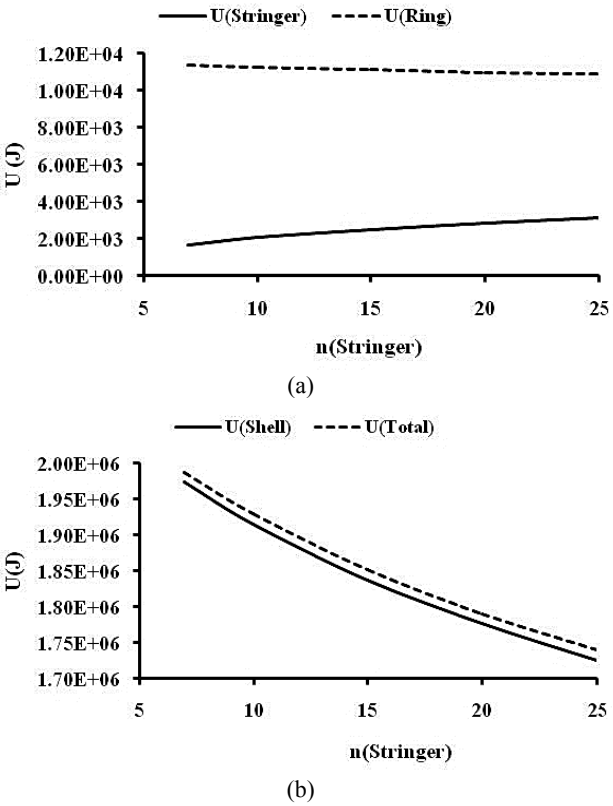

Figure 9. Changes in ring in stringer energy (a), total and shell energy (b) versus stringer number increase

Fig. 10 shows the strain energy changes versus the number of rings used in stiffened cylinder structure. As it is observable, the total energy value decreases as the number of ring rises. As the

number of rings increases, stiffness also soars; as a result, the defection decreases and therefore the strain energy is reduced too:

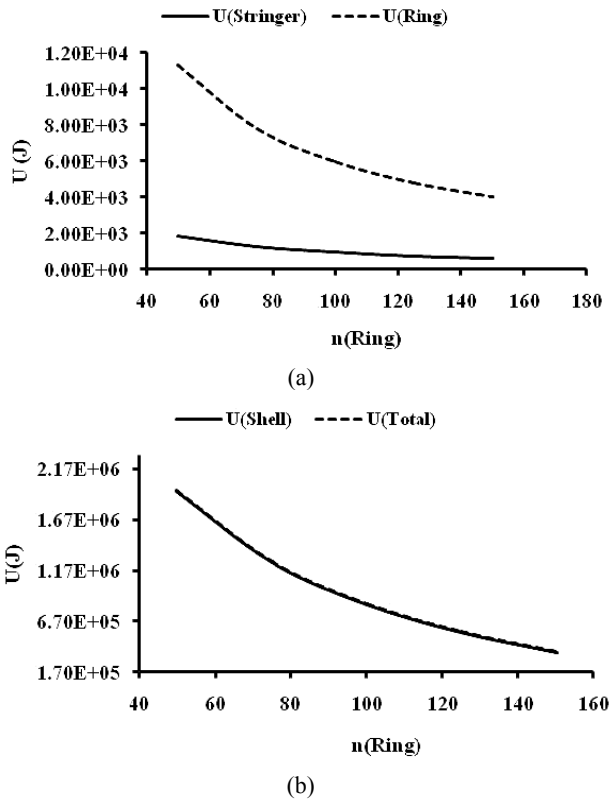

Figure 10. Changes in ring on the stringer energy (a), total and shell energy (b) versus ring number increase

Final conclusion

In this paper, the effect of various parameters (geometrical parameters, number of rings and stringers) on deflection and energy of a stiffened cylinder is investigated through analytical and numerical methods.

The stiffened cylinder is under axial loading and internal pressure, and boundary conditions for both sides of the cylinder are considered as simple supports. The following results are obtained for stiffened cylindrical composite shell:

- Deflection values in longitudinal direction of the cylinder increase by the increase in radius size.
- Deflection values in similar longitudinal positions increase as the length to radius ratio increases.
- Deflection value of similar longitudinal positions decreases as the number of rings increases, while the number of the stringers remains constant.
- Total strain energy and the strain energy created in structural elements increase by increase in the ratio of radius to thickness.
- Changes in the strain energy in longitudinal direction of the cylinder may be increasing or decreasing due to change in ratio of normalized length. Inflection point can be considered as the optimum area to determine the number of rings in order to design the stiffened cylinder.
- The energy value in stringers is increased as the number of stringers increases, while the total energy value is decreased. The total energy value has a decreasing trend by the increase in the number of rings.

References

[1] D. M. Egle, J. L. Sewall., 1989, "An analysis of the free vibration of orthogonally stiffened cylindrical shells with stiffeners treated as discrete elements", *AIAA Journal*, Vol. 6, No. 3, pp. 518-526.

[2] B. A. J. Mustafa, R. Ali,1989, "An Energy Method for Free Vibration Analysis of Stiffened Circular Cylindrical Shells", *Computer and Structures*, Vol. 32, pp. 355-363.

[3] Y. W. Kim, Y. S. Lee, 2002, "Transient analysis of ring stiffened composite cylindrical shells with both edge clamped", *Journal of Sound and Vibration* (Elsevier), Vol. 252, No. 1, pp.1-17.

[4] Karagiozisa I. Verpoest, I. Ivens, A.W. van Vuure, B. Gonmers, P. Vendeurzen, V. Efstratiou, D. Phillips, 1995, "New developments in advanced textiles for composites," *in 4th Japan International SAMPE Symposium*, vol. 644, pp.25-28.

[5] D. Phillips, I. Verpoest, J. van Raemdonk, 1996 "3D-Knitted fabrics for sandwich panels", in *Texcomp-3*, vol. 32, pp. 23-31.

[6] T.X. Yu, X.M. Tao, K.Q.Wu,1997, "Energy absorption of cellular textile composite under impact", in *Proc. ICCE/4*, pp. 1099-1100.

[7] W. L. Herald., M. S. Anderson, J. K. Anderson, M. F. Cards,1973, "Design analysis and test of a structural prototype Viking Aeroshell", *Journal of Spacecraft and Rockets*, Vol. 10, No. 1, pp. 56-65.

[8] Farley GL.,1983, "Energy absorption of composite materials", *J Compos Mater*, Vol. 17, pp. 267–79.

[9] H. Hamada, J. C. Coppola, D. Hull, Z. Maekawa, H. Sato., 1992, "Comparison of energy absorption of carbon/E and carbon/PEEK composite tubes'. *Composites*, Vol. 23, pp. 245–52.

[10] W. Barnat, P. Dziewulski, T. Niezgoda, R.Panowicz,2011, "Application of composites to impact energy absorption", *Computational Materials Science*, Vol. 50, pp.1233–1237.

[11] M. S. HooFatt, C. Lin, D. M. Revilock Jr, D. A. Hopkins, 2003 "Ballistic impact of GLARE™ fiber– metal laminates", *Composite structures*, Vol. 61, No. 1, pp. 73-88.

[12] Z. Sun, X. Hu, S. Sun, H. Chen,2013, "Energy-absorption enhancement in carbon-fiber aluminum-foam sandwich structures from short aramid-fiber interfacial reinforcement", *Composites Science and Technology*, Vol. 77, pp. 14–21.

[13] Z. W. Wang, Y. Ping E, 2011, "Energy absorption properties of multi-layered corrugated paperboard in various ambient humidities," *Materials and Design*, Vol. 32, pp. 3476–3485.

[14] Y. Ma, T. Sugahara , Y. Yang, H. Hamada, 2015, "A study on the energy absorption properties of carbon/aramid fiber filament winding composite tube", *Composite Structures*, Vol. 123, pp. 301–311.